Journal Pre-proof

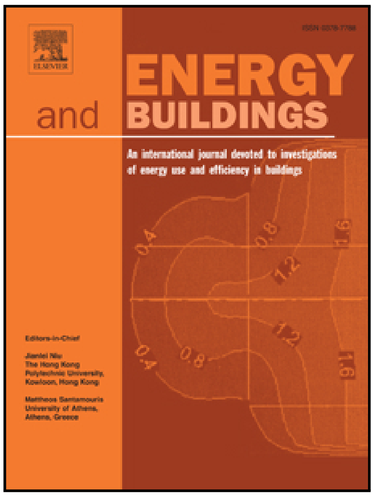

Enhancing the Accuracy of Thermal Model Calibration: Integrating Zone Air and Surface Temperatures, Convection Coefficients, and Solar and Thermal Absorptivity

M. Cecilia Demarchi, Sofía Gervaz Canessa, Gabriel Pena, Alejandro E. Albanesi, Federico Favre

PII:	S0378-7788(25)00347-0
DOI:	https://doi.org/10.1016/j.enbuild.2025.115617
Reference:	ENB 115617

To appear in: *Energy & Buildings*

Received date:	19 December 2024
Revised date:	14 February 2025
Accepted date:	13 March 2025

Please cite this article as: M. Cecilia Demarchi, Sofía Gervaz Canessa, Gabriel Pena, Alejandro E. Albanesi, Federico Favre, Enhancing the Accuracy of Thermal Model Calibration: Integrating Zone Air and Surface Temperatures, Convection Coefficients, and Solar and Thermal Absorptivity, *Energy & Buildings* (2025), doi: https://doi.org/10.1016/j.enbuild.2025.115617

Highlights

- A methodology for calibrating building thermal simulation models is presented
- Considers convection coefficients and thermal and solar absorptivity in the models
- Includes the minimization of errors in surface temperatures and air temperatures
- The accuracy of a detailed calibration is compared to a simple calibration with RMSE
- The detailed calibration greatly reduces RMSE of air and surface temperatures

Graphical Abstract

Enhancing the Accuracy of Thermal Model Calibration: Integrating Zone Air and Surface Temperatures, Convection Coefficients, and Solar and Thermal Absorptivity

M. Cecilia Demarchi,Sofía Gervaz Canessa,Gabriel Pena,Alejandro E. Albanesi,Federico Favre

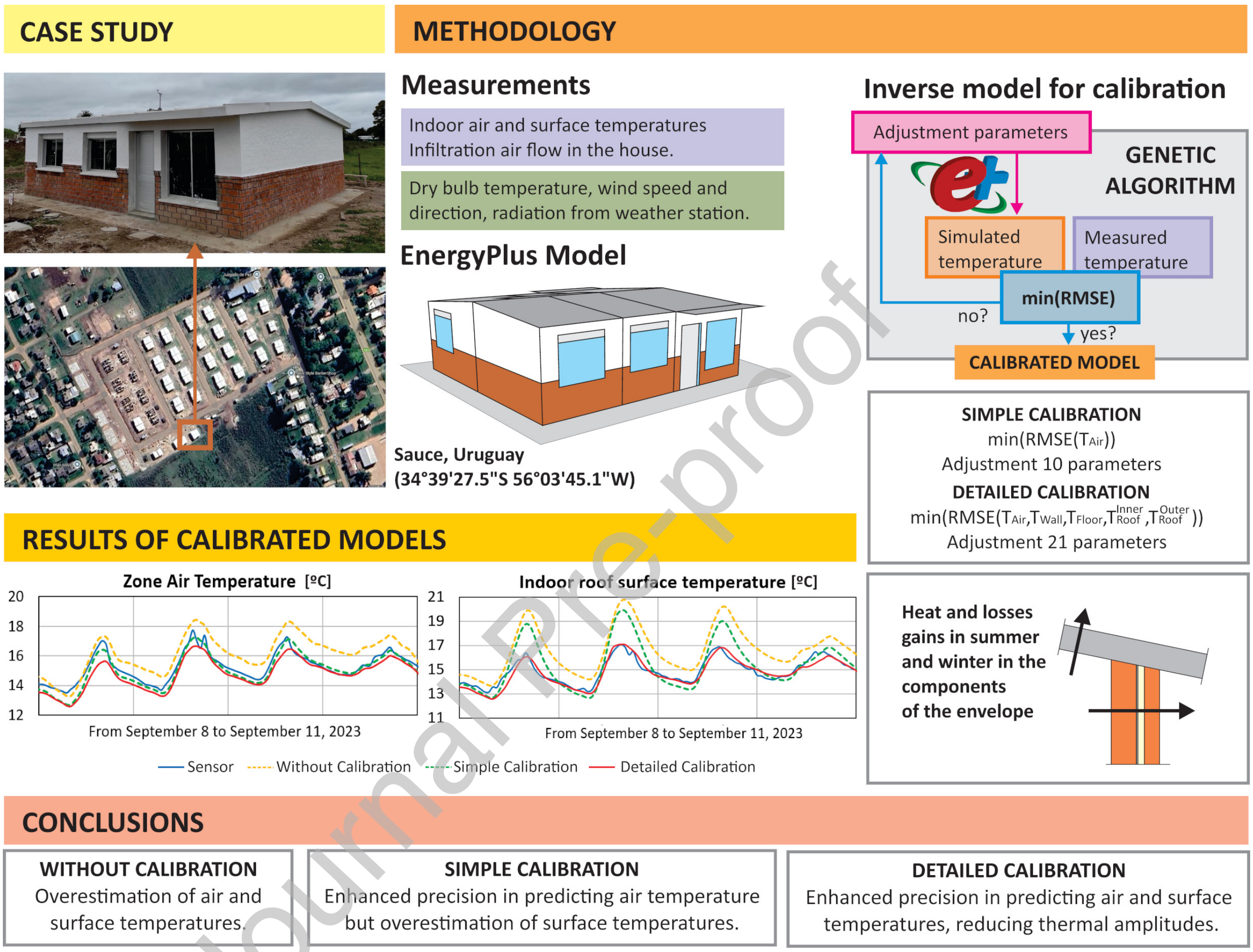

Fig. 1: Graphical abstract.

Enhancing the Accuracy of Thermal Model Calibration: Integrating Zone Air and Surface Temperatures, Convection Coefficients, and Solar and Thermal Absorptivity

M. Cecilia Demarchi[a], Sofía Gervaz Canessa[b], Gabriel Pena[b], Alejandro E. Albanesi[a] and Federico Favre[b,*]

[a]CIMEC Centro de Investigación de Métodos Computacionales, CONICET-UNL, Col. Ruta 168 s/n, Predio CONICET Santa Fe, Santa Fe, 3000, Argentina
[b]IIMPI Instituto de Ingeniería Mecánica y Produción Industrial, Julio Herrera y Reissig 565, Montevideo, 11300, Uruguay

ARTICLE INFO

Keywords:
Thermal model calibration
Convective coefficients
Solar absorptivity
Thermal absorptivity
EnergyPlus
Genetic algorithms

ABSTRACT

Building energy simulation models are indispensable tools for predicting thermal and energy performance and evaluating building energy efficiency. However, in the calibration and sensitivity analysis of these models, most studies focus on air temperatures or energy consumption, typically not taking into account critical parameters such as surface temperatures, convective heat transfer coefficients, and thermal and solar absorptivities. In this context, this work complements prior studies by incorporating these critical parameters, including convection coefficients and thermal and solar absorptivity, enhancing both the reliability and completeness of building simulation models. Using a monitoring period, air and surface temperature data were collected under free-floating conditions and supplemented with meteorological records from an on-site station. Optimization was performed using the root mean square error (RMSE) metric to minimize discrepancies between measured and simulated values of zone air and surface temperatures. The results demonstrate that the detailed calibration strategy, which considers convective coefficients and material absorptivities as design variables and minimizes errors in both air and surface temperature predictions, significantly enhances model accuracy. This approach reduces the RMSE of air temperature predictions by 60% and the RMSE of surface temperature predictions by 73% (walls), 79% (inner roof), 42% (outer roof), and 82% (floor). Further analysis of heat gains and losses emphasizes the critical role of these parameters in the accuracy in the modeling of building-environment interactions. This detailed and robust approach ensures a more precise and reliable simulation model, highlighting the critical role of advanced calibration techniques in optimizing building energy performance simulations.

1. Introduction

The current global energy crisis, defined by rising demand and the need to reduce greenhouse gas emissions, has spurred the development of "green" technologies [30]. Among the key contributors to energy consumption, building construction stands out due to its significant impact during both execution and use. Addressing this requires effective design and the application of efficient construction techniques, materials, and air conditioning systems. In this context, building energy simulation (BES) models have emerged as indispensable tools for predicting thermal and energy performance and evaluating energy efficiency strategies [37]. However, reliable results demand the calibration of parameters with high uncertainty or unknown values, narrowing the "performance gap" between measurements and simulations [8] and enhancing model accuracy [43].

The computational models used to evaluate thermal and energy performance integrate data on geometry, materials, user behavior, equipment, lighting and weather conditions. These factors determine thermal loads, airflows from infiltration and ventilation, and Heating, Ventilation, and Air Conditioning (HVAC) system performance. Popular tools for these simulations include EnergyPlus [18], TRNSYS [50], and DOE2 [14]. However, uncertainties in building data quality, quantity, and inherent model simplifications often lead to discrepancies between simulations and reality, emphasizing the need for robust calibration methods [51].

Model calibration aims to determine characteristics or parameters of the building envelope, occupancy patterns, or HVAC systems by minimizing the difference between simulation results and measured data. This process generally involves four steps: (i) data collection and uncertainty assessment for building-related parameters (e.g., geometry, orientation, material properties, infiltration rates, and soil properties), occupancy-related parameters (e.g., schedules, equipment, lighting, and HVAC systems), and air conditioning equipment properties; (ii) defining adjustment parameters, often guided by sensitivity analysis techniques like the Morris method [49, 34, 55, 54], SOBOL [4, 5], Monte Carlo simulations [23], and Pearson's chi^2 test [9]; (iii) determining parameter values through calibration methods such as manual [45, 15, 25, 10] or automated approaches [9, 52, 49, 1, 55, 43, 4, 5], Bayesian calibration [8], optimization algorithms (e.g., Genetic Algorithms (GA) [49, 55, 39, 43, 4, 32, 44, 10, 5], pattern-based searches [54], and hybrid algorithms [34]), or metamodel-based techniques [29]; and (iv) validation using metrics like coefficient of variation of the root mean square error (CV RMSE), normalized mean bias error (NMBE), root mean square error (RMSE), R-squared (R^2), mean absolute error (MAE), and goodness of

*Corresponding author
ffavre@fing.edu.uy (F. Favre)
ORCID(s):

List of abbreviations

BES	Building energy Simulation
TMY	Typical meteorological year
RMSE	Root mean square error
CV(RMSE)	Coeff. of variation of the root mean square error
NMBE	Normalized mean bias error
MAE	Mean absolute error

List of symbols

R_i	Air gap thermal resistance of facade i
ρ_{brick}	Brick Density
k_{brick}	Brick thermal conductivity
α_T	Thermal absorptance
α_S	Solar absorptance
ρ_S^G	Ground Solar reflectance
k_{EPS}	Insulation material conductivity (EPS)
ρ_{EPS}	Insulation material density (EPS)
C_{inf}	Correct. coeff. for the air permeability of the house
F_{floor}	Correct. coeff. for the ground thermal resistance
D_{glass}	Glass Dirty Coefficient
m	Mc Adams coeff. for external convection correlation
n	Mc Adams coeff. for external convection correlation
h_i^s	Internal convection coefficient walls
h_i^w	Internal convection coefficient windows
h_i^r	Internal convection coefficient roof
T_{Air}	Zone air temperature
T_{Floor}	Inner floor surface temperature
T_{Wall}	Inner wall surface temperature
T_{Roof}^{Inner}	Inner roof surface temperature
T_{Roof}^{Outer}	Outer roof surface temperature
T_{db}	Dry bulb temperature
T_s	Simulated temperature
T_m	Measured temperature
$(\overline{T_m})$	Mean of measured temperature
IR_h	Infrared radiation
ε_{sky}	Sky emissivity
σ	Stefan-Boltzman constant
θ	Angle between surface and direction of wind
V_{wind}	Wind velocity
V_{loc}	Local wind velocity
ΔP	Pressure difference

fit function (GOF), following standards such as ASHRAE Guideline 14 [27], IPMVP [19], or Federal Energy Management Program guidelines [17].

Calibration methodologies often focus on variables like energy consumption [52, 31, 53, 1, 8, 33, 46, 28] and air temperature [48, 2, 23, 6, 16, 55, 43, 25, 24, 44, 36]. Some studies extend this to include relative humidity or CO_2 generation [45, 34, 35]. Adjustment parameters typically target building envelope properties (e.g., thickness, conductivity, density, specific heat, U-value of glazing, and solar heat gain coefficient), user behavior (e.g., schedules, equipment, and lighting loads), and HVAC characteristics. While these approaches improve simulation accuracy, the inclusion of numerous variables amplifies uncertainty in the results. Other works prioritize temperature and relative humidity as calibration variables [9, 49, 15, 3, 39, 4, 10, 32, 5]. In such cases, air temperature is often the primary comparison variable, and the surface temperatures of the building envelope are generally not taken into account, leaving a significant gap in improving the reliability of thermal models.

Few investigations address calibration using temperatures under free-floating conditions, and these are typically limited to air temperatures in the zones. Most thermal calibration studies prioritize adjustments related to building envelope properties, such as density, thermal conductivity, U-value of glazing, and solar heat gain coefficient (SHGC). Air infiltration rates and convective models are occasionally considered to refine simulations. To date, no studies have incorporated the convective heat transfer coefficient (h) or the thermal and solar absorptivity of materials as design variables, which significantly reduces the accuracy of thermal models [20, 26, 22].

Building on these observations, this study aims to address the critical gaps identified in prior research by adopting a novel approach that incorporates surface temperatures and additional material properties, such as thermal and solar absorptivity and convective coefficients, into the calibration process. This expanded methodology is applied to a residential building in Sauce, Uruguay, providing a comprehensive evaluation of its effectiveness. The study compares two distinct calibration methodologies: the first employs a single-objective optimization model focused solely on air temperature, while the second extends the scope by incorporating a multi-objective optimization that simultaneously optimizes air and surface temperatures. Employing a Genetic Algorithm for its robust handling of numerous variables, speed, and flexibility, the second approach offers an efficient and precise solution to the challenges highlighted in previous studies.

This manuscript is organized as follows: Section 2 describes the methodology, including the case study, the monitoring system, the computational model, and the calibration methodology. Section 3 presents the numerical results and the discussion of those results. Finally, Section 4 provides the conclusions of the study.

2. Methodology

Based on the outlined approach, the general methodology of the study involves the following steps: (i) selecting the house for analysis, reviewing architectural plans, and conducting on-site verification of construction details; (ii) monitoring indoor air temperature, interior and exterior surface temperatures of walls, roof, and floor, as well as air permeability through a blower door test; (iii) creating a weather file using monitored ambient temperature, solar irradiation (on vertical and horizontal planes), and wind data (speed and direction) from a nearby meteorological station; (iv) developing the computational model in EnergyPlus; (v) implementing and comparing two calibration strategies, one simple and one detailed, both based on Genetic Algorithms; and (vi) analyzing and discussing the results.

2.1. Case study

The case study focuses on a residential house located in a rural neighborhood in Sauce, Uruguay (34°39’27.5"S, 56°03’45.1"W), as shown in Figure 2. The house includes a living room and kitchen area, three bedrooms, and one bathroom, with its facade oriented to the northwest, as detailed in the floor plan and a 3D view in Figure 3. The building envelope consists of an exterior vertical wall, and a gabled roof, as depicted in Figure 4.

Fig. 2: Satellite image of the cite during construction.

The interior layer includes a 12 cm clay brick, followed by a 1 cm waterproofing layer composed of sand, Portland cement with waterproofing additives, and a bituminous emulsion. This is covered by 3 cm of expanded polystyrene insulation (EPS), a 1 cm air gap, and a 5.5 cm exterior clay brick layer. Interior walls are constructed from 12 cm clay bricks with a rough white finish on both sides.

The building envelope features an exterior vertical wall assembly composed of a 22 cm double-wall structure. The lower 1.10 m of the exterior surface consists of exposed brick, while the area above that height has a rough white finish. The roof is gabled, with the ridge centered over the house and a slight slope towards the front and rear facades. It consists of a panel made of double-layer white metal sheeting with a 15 cm core of expanded polystyrene insulation. The floor comprises a 12 cm thick concrete slab finished with white granite-patterned ceramic tiles featuring gray veining. The bathroom ceiling is formed by a 10 cm thick concrete slab, finished with white paint.

Regarding openings, the kitchen-living area features a sliding window on the facade measuring 1.80 m in height and 1.60 m in width, and another window on the rear facade measuring 1.15 m in height and 1.50 m in width. The bedrooms have sliding windows measuring 1.15 m in height and 1.50 m in width, equipped with roller blinds for shading. The bathroom features an awning window measuring 1.15 m in height and 0.40 m in width. All openings are made of aluminum with 3 mm thick clear glass. The main entrances to the house, located on the facade and rear facade of the kitchen-living area, are aluminum doors. One door measures 0.95 m in width and 2.05 m in height, with a side panel of glass, while the other measures 0.80 m in width and 2.05 m in height, featuring a 3 mm clear glass panel in the upper half. Interior doors are wooden panels measuring 0.80 m in width and 2.05 m in height.

2.2. Monitoring System

The house was monitored over 17 days, from September 7, 2023, to September 23, 2023, immediately after construction was completed but before being occupied. During the measurement period, the house remained unoccupied, with blinds raised, interior doors open, and windows closed, meaning the indoor temperature depended solely on the envelope materials and their interaction with the environment. Figure 5 shows the approximate placement of the sensors.

During this time, indoor air temperature and relative humidity in the kitchen-living area were monitored using two Hobo UX100-003 sensors, placed at a height of 170 cm above the floor and distributed within the room. These sensors were configured to collect data every 15 minutes and have an uncertainty of ±0.21°C for temperature and ±3.5% for relative humidity. To compare the zone temperature obtained from the model with the measurements, a single calibration temperature (T_{Air}), representing the average of the sensor readings, was considered. This approach is valid because the temperature difference between sensors is less than 1ºC and only occurs at peak values.

Simultaneously, surface temperatures of selected envelope components were recorded, including T_{Floor}, T_{Wall}, T^{Inner}_{Roof}, and T^{Outer}_{Roof}. These were measured with platinum resistance sensors (PT1000, ±0.25°C uncertainty) connected to a DataTaker DT 80M datalogger.

Reliable and complete data were obtained during the measurement period for the weather station, Hobo sensors, and wall and floor thermocouples. However, roof temperature measurements were only available from September 7, 2023, to September 14, 2023.

Air permeability was determined through a blower door test performed at the main entrance of the house. The test followed ISO 9972:2015 standards, using a TEC Minneapolis Blower Door Model 4 in depressurization mode. Ten data points of airflow and pressure differential (ranging from 18 to 85 Pa) between the interior and exterior were recorded. The test indicated an airflow of 756 m^2h^{-1} (±4,2%) at a pressure difference of 50 Pa, corresponding to an air exchange rate (n_{50}) of 5.21 h^{-1}.

To generate the climate file, a weather station was installed near the study house. The station monitored dry-bulb temperature (using PT1000 sensors with ±0.25°C uncertainty) and global solar radiation on horizontal and vertical planes oriented north (measured with a Licor 200R photovoltaic sensor with ±5% uncertainty). Data acquisition was performed with a DataTaker DT 80M datalogger. Wind data (speed and direction) and wet-bulb temperature were obtained from nearby third-party meteorological stations managed by state authorities. Missing data were supplemented with records from nearby meteorological stations (San Jacinto and Carrasco) between August 1, 2023, and September 6, 2023, to avoid simulation errors caused by thermal inertia effects.

Infrared radiation was calculated to complete the meteorological file using the model proposed in the EnergyPlus documentation (Equation 1), where T_{db} is the dry bulb temperature, (T_{dp}) is the dew point temperature, σ is the Stefan-Boltzmann constant, and ε_{sky} is the sky emissivity determined by Clark and Allen (Equation 2).

$$IR_h = \varepsilon_{sky}\sigma T^4_{db} \tag{1}$$

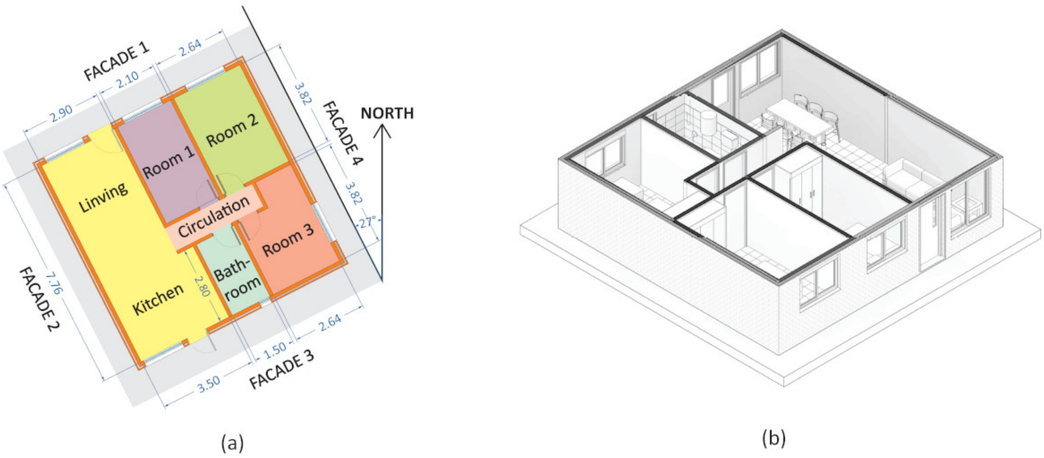

Fig. 3: Geometry of the building under study.

Fig. 4: Exterior envelope of the building under study.

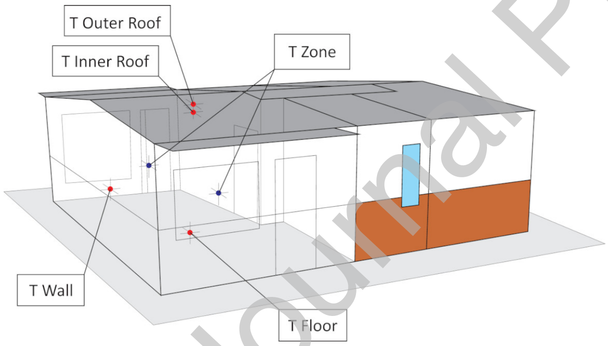

Fig. 5: Sensor distribution. Blue markers indicate Hobo sensors measuring T_{air}, and red markers indicate thermocouples measuring T_{surf}.

$$\varepsilon_{sky} = 0.787 + 0.764 \ln\left(\frac{T_{dp}}{273}\right) \tag{2}$$

2.3. Computational Model

The thermal simulation model is created and configured to run on EnergyPlus v.23.2. Based on technical documentation and on-site measurements, the geometry is defined, and appropriate materials are assigned to each element. To ensure the simulation is as accurate and representative as possible, each space is assigned to a separate zone: ZONE 1: kitchen-living area; ZONE 2: bedroom 1; ZONE 3: bedroom 2; ZONE 4: bedroom 3; ZONE 5: bathroom; ZONE 6: bathroom ceiling; and ZONE 7: corridor. Since the house features an exposed brick baseboard and white-painted walls, external surfaces are divided into two sections to account for their differing behaviors. Similarly, to consider the temperature increase caused by radiation entering through the window, the kitchen floor is divided into two sections, as the sensor is positioned to avoid direct exposure to the radiation.

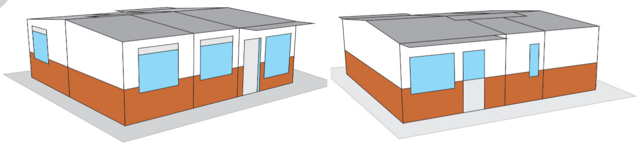

Fig. 6: Computational model.

Regarding algorithms, the ConductionTransferFunction is used for heat transfer in walls and roofs, while the F-Factor method is applied for heat transfer between the ground and the floor, where the surface temperature is taken from the weather file.

Air infiltration flow is configured using the results from the blower door test. The flow for each component i is based on Equation 3:

$$\dot{m}_i(kg/s) = C_i \Delta P_i^n \tag{3}$$

where coefficients C_i and n_i are initially based on theoretical values proposed by [42]. These values are adjusted using a proportionality factor to ensure that the total flow for a pressure difference of $\Delta P = 50\,Pa$ matches the measured value from the test. The adjusted coefficients are then integrated into the model using the "AirFlowNetwork" block, which considers air inflow through these spaces and the interaction between zones.

Considering the monitoring conditions and dust deposits carried by the wind during construction, a corresponding dirt value is applied to the glazing properties.

	Value range	
Acronym	Case 2	Case 3
α_s	–	0.01 - 0.99
α_t	–	0.01 - 0.99
D_{glass}	0.50 - 1.00	0.50 - 1.00
$\rho_{brick}(kg/m^3)$	–	800 - 2000
$k_{EPS}(W/mK)$	0.01 - 0.10	0.01 - 0.10
$\rho_{EPS}(kg/m^3)$	5.00 - 15.00	5.00 - 15.00
$R_i(m^2K/W)$	0.01 - 1.00	0.01 - 1.00
C_{inf}	0.00- 2.00	0.00 - 2.00
F_{floor}	0.1 - 2.00	0.1 - 2.00
ρ_S^G	0.01 - 0.5	0 .01 - 0.5
m_{wall}	–	1.00 - 10.00
n_{wall}	–	1.00 - 10.00
m_{roof}	–	1.00 - 10.00
n_{roof}	–	1.00 - 10.00
$h_i(W/m^2K)$	–	0.10 - 20.00

Table 1
Parameters and variation ranges.

Given the handcrafted nature of the construction, discrepancies between theoretical and actual values for material properties and air gaps in walls are addressed by defining air thermal resistances.

Based on these considerations, the following three cases are defined:

Case 1. This case uses thermal and optical material properties obtained from the literature. Air thermal resistances (R_i) are set to 1 m^2K/W, and the dirt coefficient for glazing is set to 1, corresponding to clean glass. Infiltration coefficients from the blower door test are applied, and the "Adaptive Convection Algorithm" is used to calculate both interior and exterior convective coefficients.

Case 2. Based on Case 1, this model incorporates calibration of material thermal properties, R_i, D_{glass}, infiltration coefficients adjusted using C_{inf}, ρ_S^G, and floor conductivity adjusted by F_{floor}. Each parameter is constrained within the ranges shown in Table 1. In this case, calibration minimizes the differences between measured and simulated T_{Air} in the zone using single-objective optimization.

Case 3. Also based on Case 1, this model considers the adjustment variables mentioned in Case 2, modifies the convection models, and incorporates additional calibration parameters. These include internal convective coefficients (h_{wall}, h_{roof}, h_{floor}) and h_{glass}, and external coefficients (calculated using the McAdams model [38]), as well as the thermal and solar absorptivity (α_T and α_S) of walls, floors, and roofs, both interior and exterior, within the ranges shown in Table 1.

The inclusion of convective coefficients in the calibration process is justified by the findings of [26], which demonstrate the significant impact of these coefficients on the thermal performance of buildings, particularly for the same typology and climate as the present study. On the other hand, the consideration of thermal and solar absorptivity parameters is based on the results of [23, 22]. Specifically, the sensitivity analysis presented in [22] highlights absorptivity as a key parameter influencing the thermal behavior of the studied typology.

Unlike Case 2, this calibration adopts a multi-objective approach, minimizing not only the differences in T_{Air} but also T_{Floor}, T_{Wall}, T_{Roof}^{Inner}, and T_{Roof}^{Outer} simultaneously.

For the internal convective coefficients (h_{wall}, h_{roof}, h_{floor} and h_{glass}), constant values are assumed within a range shown in Table 1. For external surfaces, the convective coefficient is calculated using the McAdams model [38], as expressed in Equation 4:

$$h_{ext} = mV_{loc} + n \tag{4}$$

This model accounts for surface geometry, roughness, angle relative to wind direction, and local wind velocity (V_{loc}). For roofs with an inclination of less than 45°, V_{loc} is taken as the wind velocity. For walls, V_{loc} depends on orientation.

For surfaces facing the wind, where $0° < \theta \leq 10°$:

$$V_{loc} = \begin{cases} 0.15V_{wind} & \text{for } V_{wind} \leq 1\,m/s, \\ 0.5\,m/s & \text{for } 1 < V_{wind} \leq 2\,m/s, \\ 0.25V_{wind} & \text{otherwise.} \end{cases} \tag{5}$$

or, where $10° < \theta \leq 90°$:

$$V_{loc} = V_{wind}\sin\theta \tag{6}$$

and, when $90° < \theta \leq 180°$:

$$V_{loc} = 0.25V_{wind}\sin\theta \tag{7}$$

The coefficients m and n (for both roofs and walls) are proposed as adjustment variables within a range shown in Table 1.

2.4. Calibration Methodology

The calibration of Cases 2 and 3 is performed using an automated, iterative inverse model coupled with EnergyPlus for thermal simulation. This approach is complemented by a stochastic optimizer, specifically a Genetic Algorithm, aimed at identifying the optimal set of variables that minimize the discrepancies between air temperatures in the zones and the surface temperatures, both interior and exterior, of walls and roofs.

For Case 2, a single-objective optimization is proposed using the algorithm proposed by Deep [13], implemented within Distributed Evolutionary Algorithms in Python (DEAP) [21]. The optimization process starts with a random sample using the design variables from Section 2.3 with the ranges detailed in the second column of the Table 1. The thermal performance is evaluated using EnergyPlus. This data set is fed to GA, which evaluates the results and generates a new data set. This sequence is repeated iteratively until the algorithm converges.

For the multi-objective optimization used in Case 3, the Non-Dominated Sorting Genetic Algorithm II (NSGA-II) [11, 12] implemented in pyOpt v1.2.0 [47] has been used. NSGA-II is an evolutionary multi-objective optimization algorithm designed to identify optimal solutions in problems where multiple fitness functions must be minimized. It starts with a random population, using the design variables from Section 2.3 with the ranges detailed in the third column of the Table 1, which obtains the thermal efficiency with EnergyPlus. This sample is evaluated using the dominance criterion that establishes that a solution is superior to another if it is equal or better in all objectives and strictly better in at least one. It calculates a crowding distance to maintain diversity. Solutions are selected favoring those with the best result and greatest separation. New solutions are generated that are combined with the previous population. The process is repeated until a well-distributed optimal solution is reached.

To avoid local minima in both mono-objective and multi-objective optimization, variation and recombination operators are applied to the population throughout the optimization process. These operators include mutation, which introduces modifications to selected solutions; crossover, which combines elements from different solutions to generate new candidates; and reproduction, where selected solutions are carried forward without alteration. These mechanisms ensure diversity within the population and enhance the algorithm's ability to explore the design space effectively.

With the aim of penalizing large errors and avoiding deviations of the model from reality [7], the RMSE index (root mean square error, see Eq. 8) is used to quantify this difference, with calibration considered precise when the RMSE value is below 1ºC. In Case 1, the optimization is single-objective, minimizing T_{Air}, whereas in Case 2, it is multi-objective, simultaneously minimizing T_{Air}, T_{Floor}, T_{Wall}, T_{Roof}^{Inner}, and T_{Roof}^{Outer}.

$$RMSE = \sqrt{\frac{\sum (T_s - T_m)^2}{n}} \tag{8}$$

To complete the evaluation of results uses CV(RMSE) Eq. 9, NMBE Eq. 10, and MAE Eq. 11, which provide insights into the accuracy of the calibration.

$$CV(RMSE) = 100 \frac{\sqrt{\frac{\sum (T_s - T_m)^2}{n}}}{\overline{T_m}} \tag{9}$$

$$NMBE = 100 \frac{\sum (T_s - T_m)}{n\overline{T_m}} \tag{10}$$

$$MAE = \frac{\sum |T_s - T_m|}{n} \tag{11}$$

In all indicators, T_s represents the simulated temperature, T_m the measured temperature, $\overline{T_m}$ the mean of measured temperatures, and n the number of measurements. According to ASHRAE Guideline 14 [40], a model is considered calibrated when the NMBE is within ±10% and the CV(RMSE) is within ±30% for hourly values [41].

Case	Zone	Wall	Inner Roof	Outer Roof	Floor
Case 1	1.17	2.24	2.33	5.44	1.91
Case 2	0.36	0.88	1.30	5.40	0.50
Case 3	0.47	0.60	0.48	3.17	0.34

Table 2
RMSE (ºC)

Case	Zone	Wall	Inner Roof	Outer Roof	Floor
Case 1	7.45	14.62	16.04	44.43	12.65
Case 2	2.33	5.78	8.98	44.08	3.34
Case 3	3.00	3.92	3.29	25.78	2.28

Table 3
CV(RMSE) %

Case	Zone	Wall	Inner Roof	Outer Roof	Floor
Case 1	6.55	13.73	13.60	29.07	10.14
Case 2	-0.04	4.73	4.22	29.92	2.42
Case 3	-1.82	2.80	0.28	12.87	0.06

Table 4
NMBE %

Case	Zone	Wall	Inner Roof	Outer Roof	Floor
Case 1	1.04	2.10	1.97	3.94	1.52
Case 2	0.31	0.74	0.89	3.92	0.41
Case 3	0.38	0.49	0.38	2.23	0.30

Table 5
MAE(ºC)

3. Results and Discussion

This section presents and discusses the results obtained using the proposed error metrics and the comparison between measured and simulated temperatures for each case after calibration. Additionally, the values of the adjustment variables are detailed, and the cases are compared. Finally, a heat flow balance is performed, and the observed differences are analyzed.

3.1. Error Metrics

This subsection presents and analyzes the results for Cases 1, 2, and 3, comparing the simulation outputs with the measurements recorded by the sensors. The comparisons are made using the statistical indicators RMSE (Table 2), CV(RMSE) (Table 3), NMBE (Table 4), and MAE (Table 5), whose values are detailed below.

Based on the results obtained from post-calibration simulations and considering the RMSE values, the metric used for optimizations, it is evident that temperature differences are significantly reduced after both calibrations. This indicates that the temperatures calculated by the calibrated models are more accurate compared to Case 1. When analyzing the RMSE values for T_{Air}, Case 2 achieves an error of 0.36ºC, and Case 3 an error of 0.47ºC, while for Case 1, the error is 1.17ºC. This demonstrates that after calibration, the accuracy in predicting T_{Air} improves. For surface temperatures, as shown in Table 2, the RMSE values for Case 2 are higher than those for Case 3, particularly for T_{Floor}, T^{Inner}_{Roof}, and T^{Outer}_{Roof}. This behavior suggests that the Case 3 model provides a more accurate representation of the building, significantly improving temperature predictions.

Regarding CV(RMSE), following the RMSE trend, the CV(RMSE) for T_{Air} in Cases 2 and 3 are 2.33% and 3.00%, respectively, compared to 7.45% for Case 1. Moreover, these values are well below the limits established by ASHRAE Guideline 14.0 (±30%), indicating that all three models are good representations of reality, with Cases 2 and 3 offering higher precision. For CV(RMSE) corresponding to surface temperatures, as shown in Table 3, the errors are up to five times lower than those of Case 1, with Case 3 achieving errors around 3%, except for T^{Outer}_{Roof}, making it the most precise case.

When examining the NMBE and MAE indicators detailed in Tables 4 and 5, a consistent trend with the previously analyzed errors is observed: while Case 2 shows a lower error for zone temperatures, Case 3 achieves significant improvements in predicting surface temperatures.

In summary, the results suggest that using RMSE as an optimization criterion allows for satisfactory calibration outcomes. Furthermore, it is concluded that the Case 3 model demonstrates greater precision and reliability in thermal simulation, as it exhibits the lowest errors for both air and surface temperatures.

3.2. Temperature Comparisons

The air and surface temperatures obtained for each case during the calibrated periods mentioned in Section 2.4 are compared below.

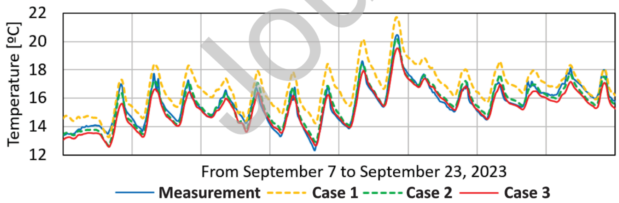

Fig. 7: Comparison of T_{Air}.

Analyzing T_{Air} as shown in Figure 7, the simulation results for Case 1 overestimate the measured air temperature, while Cases 2 and 3 provide a closer approximation.

For T_{Wall}, as shown in Figure 8, the temperatures from Case 1 exceed measured values by an average of 2ºC, whereas the results from the calibrated cases are more accurate, with Case 3 offering the highest precision. This behavior is similarly observed for T_{Floor}, shown in Figure 9.

When comparing T^{Inner}_{Roof}, the values obtained in Cases 1 and 2, as shown in Figure 10, fail to accurately reproduce

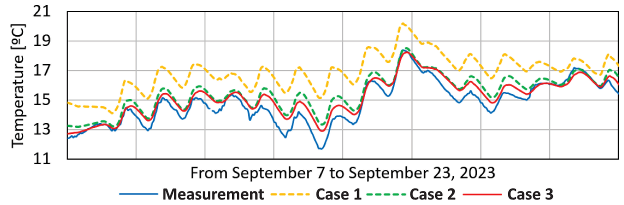

Fig. 8: Comparison of T_{Wall}.

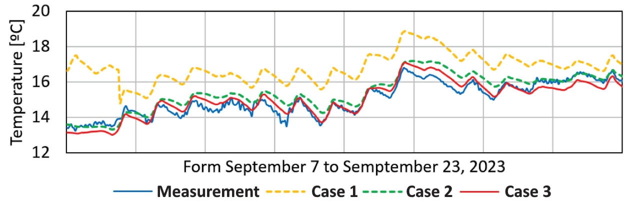

Fig. 9: Comparison of T_{Floor}.

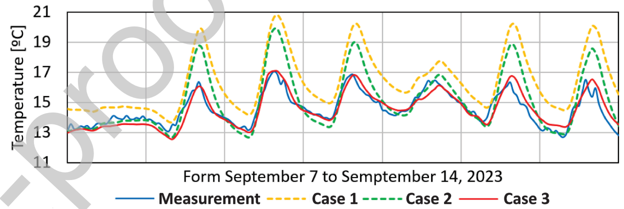

Fig. 10: Comparison of T^{Inner}_{Roof}.

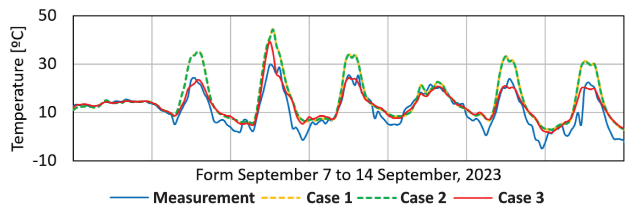

Fig. 11: Comparison of T^{Outer}_{Roof}.

the measured temperatures, with differences exceeding 4ºC at peak values. In contrast, Case 3 exhibits much greater accuracy, effectively capturing the building's thermal amplitudes.

Examining T^{Outer}_{Roof} in Figure 11, a similar trend to T^{Inner}_{Roof} is observed, with temperature differences exceeding 10ºC. The results for Cases 1 and 2 are nearly identical, while Case 3 achieves higher precision, mirroring its performance for interior temperatures.

Figures 12, 13, 14, 15, and 16 show the differences between the measured and simulated temperatures for Cases 1, 2, and 3 within the considered time interval. It is observed that, except for specific moments, these differences remain within a range of ±1°C for T_{Air}, T_{Wall}, T_{Floor}, and T^{Inner}_{Roof}, and within ±5°C for T^{Outer}_{Roof}. This represents an improvement

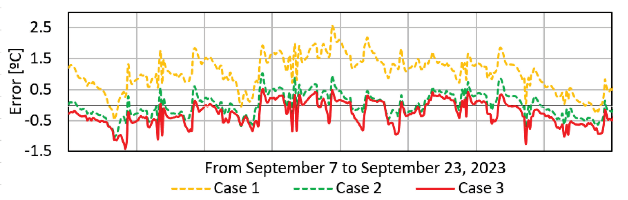

Fig. 12: Error of T_{Air}.

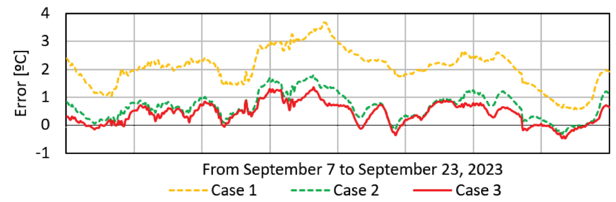

Fig. 13: Error of T_{Wall}.

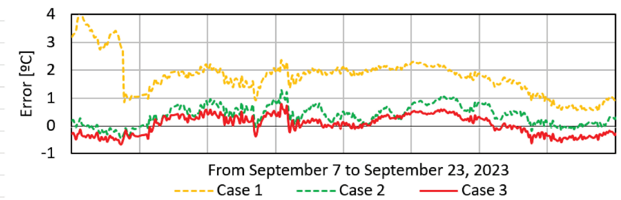

Fig. 14: Error of T_{Floor}.

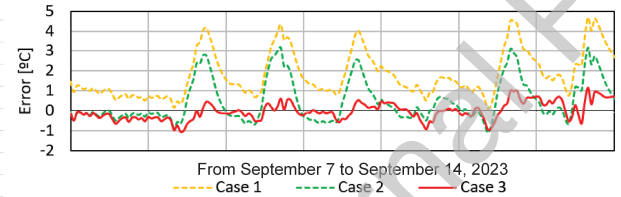

Fig. 15: Error of T_{Roof}^{Inner}.

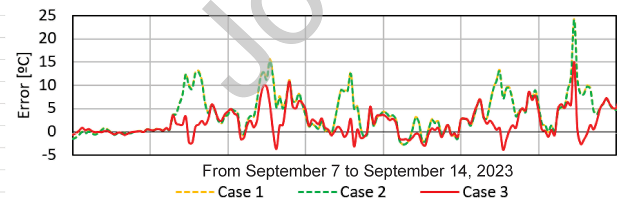

Fig. 16: Error of T_{Roof}^{Outer}.

compared to the errors obtained in Case 2, especially for the roof.

Figure 12 shows a significant reduction in the error of T_{Air} from Case 1 to Cases 2 and 3, although the errors in Case 3 are slightly higher by 0.2°C compared to Case 2. Regarding T_{Wall} and T_{Floor}, Figures 13 and 14 indicate that the errors in Cases 2 and 3 are considerably lower than in

Parameters	Case 1	Case 2	Case 3
$k_{EPS}(W/mK)$	0.04	0.0694	0.0629
$\rho_{EPS}(kg/m^3)$	15	6.9895	13.6355
$k_{brick}(W/mK)$	1300	1300	1335.6
$R_1(m^2K/W)$	1	0.4917	1.0200
$R_2(m^2K/W)$	1	0.2377	0.2593
$R_3(m^2K/W)$	1	0.3334	1.0527
$R_4(m^2K/W)$	1	0.2482	1.3571
C_{inf}	1	1.2931	2.2578
D_{glass}	1	0.6038	0.6578
F_{floor}	0.50	0.2491	0.4680
ρ_S^G	0.26	0.015	0.1717
m_{roof}	–	–	6.05
n_{roof}	–	–	5.29
n_{wall}	–	–	6.19
n_{wall}	–	–	5.72
$h_{wall}(W/m^2K)$	–	–	7.34
$h_{floor}(W/m^2K)$	–	–	9.71
$h_{roof}(W/m^2K)$	–	–	7.31
$h_{glass}(W/m^2K)$	–	–	10.33

Table 6
Values obtained for the parameters after calibration

Case 1. Additionally, for almost the entire analyzed period, the errors in Case 3 are 0.5°C lower than those in Case 2.

For T_{Roof}^{Inner}, Figure 15 shows that Case 3 keeps errors within the range of ±1°C and reduces error peaks from 4°C to values close to 0.5°C. In the case of T_{Roof}^{Outer}, no significant differences in errors are observed between Cases 1 and 2; however, in Case 3, there is a reduction in error peaks, with differences ranging from 5°C to 15°C compared to Cases 1 and 2.

These observations are consistent with the temperatures presented in Figures 7, 8, 9, 10, and 11, where Case 2 provides a better estimation of T_{Air} since the calibration focuses on minimizing the gap in this variable. In contrast, Case 3 more accurately captures not only T_{Air} but also the surface temperatures T_{Wall}, T_{Floor}, T_{Roof}^{Inner}, and T_{Roof}^{Outer}, resulting in a more precise computational model. Furthermore, Case 3 better represents the shape of the temperature curves, accurately capturing the amplitude variations observed in the measured data. This improved representation suggests that the model can reproduce not only average values but also thermal dynamics more faithfully. This trend is reflected in the RMSE and other error metrics, such as CV(RMSE), NMBE, and MAE, where the simulated temperatures after each calibration show significant improvements compared to Case 1, approaching the measured values. In particular, Case 3 consistently demonstrates greater accuracy compared to Case 2.

3.3. Adjustment Variables

Table 6 shows the differences in the adjustment variable values common to all three cases, comparing the initial values from Case 1 with those obtained after calibration for Cases 2 and 3.

Case	α_T^{Iwall}	$\alpha_T^{Owall\ red}$	$\alpha_T^{Owall\ white}$	α_T^{Ifloor}	α_T^{Iroof}	α_T^{Oroof}
Cases 1 y 2	0.93	0.93	0.93	0.90	0.25	0.25
Case 3	0.35	0.49	0.49	0.51	0.52	0.41

Table 7
Thermal absorptivity values

Case	α_S^{Iwall}	$\alpha_S^{Owall\ red}$	$\alpha_S^{Owall\ white}$	α_S^{Ifloor}	α_S^{Iroof}	α_S^{Oroof}
Cases 1 y 2	0.55	0.55	0.55	0.45	0.40	0.40
Case 3	0.40	0.54	0.37	0.32	0.51	0.31

Table 8
Solar absorptivity values

Case	h_{int}^{wall}	h_{ext}^{wall}	h_{int}^{roof}	h_{ext}^{roof}
Case 1	1.02	6.16	0.56	11.63
Case 2	0.96	6.08	0.67	11.62
Case 3	7.34	11.62	7.31	32.97

Table 9
Mean convection coefficients comparison.

Analyzing the properties related to heat conduction in the surfaces, as shown in Table 6, it is observed that the k_{EPS} obtained from the calibrations for Cases 2 and 3 is approximately 50% higher than in Case 1. Regarding the R_i values, those from Case 2 are below 0.5 m^2K/W, contrasting with Case 3, which exhibits values around 1.20 m^2K/W, except for R_2 on the façade. For the floor, F_{floor} in Case 2 is half the value obtained in Case 3. These results indicate that the obtained values lead to a lower overall thermal resistance, particularly in Case 2, which tends to reduce temperatures.

Regarding air exchange with the external environment, the C_{inf} in Case 3 is double that of Cases 1 and 2, contributing to increased cooling of the house.

For D_{glass}, both calibrations yield similar values, approximately 0.6, suggesting that dust accumulation on the glazing reduces the radiation entering the room, thereby limiting the heating of the zone air. Neglecting this effect would overestimate temperature calculations.

Finally, according to Table 6, the ρ_S^G value in Case 2 is significantly lower than that obtained in Case 3, indicating that Case 2 aims to further reduce T_{Air} compared to Case 3 by limiting heat gain from radiation.

Tables 7 and 8 compare the theoretical and calibrated values of α_T and α_S for the surfaces.

Comparing the values obtained for Case 3, the α_S coefficients are significantly lower than those in Cases 1 and 2. This indicates that the heat absorbed in Case 3 is reduced compared to the other cases, leading to lower model temperatures and better replicating the house's behavior.

For α_T, a similar trend is observed, although its influence on temperature is less pronounced compared to α_S.

Tables 9 show that the average convective coefficients obtained through calibration in Case 3, both interior and exterior, are significantly higher than those in Cases 1 and 2, which contributes to reducing temperatures. This comparison highlights the importance of calibrating this parameter, as it better adjusts surface temperatures, particularly those of the roof, both interior and exterior, achieving greater accuracy in capturing thermal amplitudes. These results suggest that the correlations proposed in EnergyPlus underestimate convective coefficients.

Analyzing the overall results, it can be concluded that the detailed calibration strategy, which includes both the consideration of convective coefficients and thermal and solar absorptivities, as well as the minimization of errors in surface temperatures in addition to air temperatures (as implemented in Case 3), leads to more accurate temperature predictions compared to the simpler approach in Case 2. This is also reflected in the values of variables common to both models. In Case 2, the global trend is to reduce overall thermal resistance and solar gain through radiation, while in Case 3, these adjustments are more precise. This improvement underscores the enhanced accuracy in temperature calculations achieved with Case 3 compared to Case 2. The results further illustrate the interdependence of parameters: in Case 2, the adjustment variables are constrained to reduce temperatures, whereas in Case 3, incorporating additional variables and altering model constraints yields values that are more precise and representative of reality.

3.4. Thermal load balance

To further analyze the differences between the models obtained using two distinct calibration methodologies, Case 2 and Case 3, an annual simulation was performed for both models. The simulation incorporated an HVAC system with a heating setpoint of 21°C and a cooling setpoint of 24°C, modeled using the EnergyPlus *IdealLoadsHVAC* system. Climatic data was based on the Typical Meteorological Year (TMY) for Montevideo, with calibration months adjusted to reflect measured data.

Thermal load balances were conducted for summer and winter periods, corresponding to December through February and June through August, respectively, in the Southern Hemisphere. These balances provide an in-depth analysis of heat gains and losses across the dwelling components.

During the summer period, the thermal energy required to maintain a temperature of 24°C is relatively similar between the two cases, with Case 3 requiring 11% more HVAC energy compared to Case 2. Despite the similarity in HVAC loads, significant differences are observed in heat transfer patterns: heat gains through windows in Case 3 are 65% higher than in Case 2, while heat gains through the roof in Case 2 are nearly ten times greater than those in Case 3. These differences result in heat losses through the floor being 69% higher in Case 3 (see Fig. 17).

During the winter period, the thermal energy required to maintain a temperature of 21°C is 30% higher in Case 3 than in Case 2. This difference is attributed to 74% greater losses through infiltration, double the losses through the floor, and 29% greater losses through the roof in Case 3. Conversely, heat losses through walls are 20% higher in Case 2 than in Case 3 (see Fig. 18).

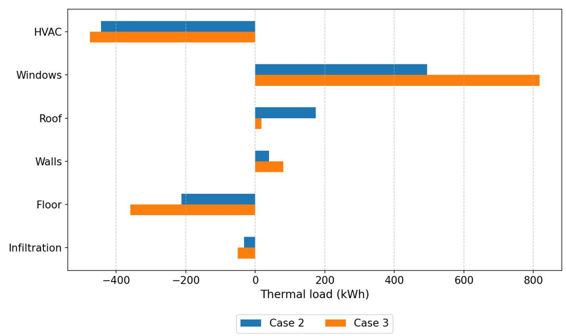

Fig. 17: Thermal loads during summer.

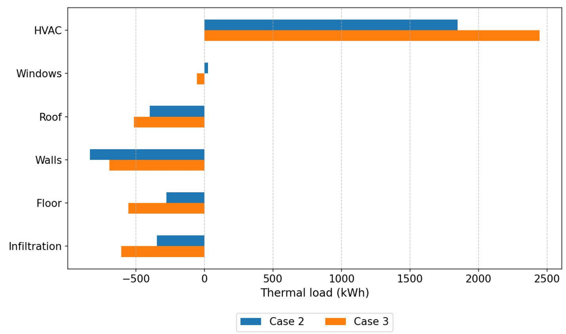

Fig. 18: Thermal loads during winter.

Anually, Case 3 requires 33% more energy from the HVAC system to maintain the setpoint temperatures than Case 2. The contrasting thermal load balances between Case 2 and Case 3 highlight the sensitivity of calibrated building energy models to the chosen methodology. These differences underscore how calibration approaches influence the representation of heat exchange dynamics with the surrounding environment. Accurately capturing these dynamics is essential for various applications of the model, including evaluating energy efficiency measures and predicting thermal performance under diverse conditions.

4. Conclusion

This study addressed the calibration of the thermal simulation model of a residential building located in Sauce, Uruguay, using an iterative inverse model that combines thermal simulation in EnergyPlus with a Genetic Algorithm (GA) to minimize the discrepancies between measured and simulated temperatures. Over a 17-day period, air and surface temperatures of the building envelope were monitored under free-floating conditions, complemented by meteorological data from an on-site station to generate the climate file.

Two calibration approaches were evaluated: a simple approach (Case 2), commonly used in the literature, focused on adjusting variables related to material properties, air thermal resistances, infiltration, and glass dirtiness; and a detailed approach (Case 3), which incorporated internal and external convection coefficients, advanced convection models, and the thermal and solar absorptivities of exposed materials. Optimization was conducted using the root mean square error (RMSE) metric, considering only zone air temperature in Case 2 and both air and surface temperatures (roof, floor, and walls) in Case 3.

The results demonstrate that incorporating surface temperatures, convective heat transfer coefficients, and thermal and solar absorptivities as design variables, along with the use of multi-objective optimization, significantly improves model accuracy. In Case 2, the RMSE of air temperature predictions decreases by 69%, while the RMSE of surface temperatures predictions decreases by 60% (walls), 45% (inner roof), 1% (outer roof), and 84% (floor). Case 3, representing the more detailed model, achieves even greater accuracy, with RMSE reductions in surface temperature predictions of 73% (walls), 79% (inner roof), 42% (outer roof), and 82% (floor). However, for air temperature predictions, Case 2 outperforms Case 3, with a 69% RMSE reduction compared to 60% in the latter. This difference arises because Case 2 employs a single-objective optimization focused exclusively on air temperature, whereas Case 3 adopts a multi-objective optimization approach that simultaneously considers air temperature, surface temperatures, convective heat transfer coefficients, and thermal and solar absorptivities. All of the above suggests that Case 3 is a more detailed representation of the thermal interactions between the building and its environment.

The comparative analysis of thermal load balances between Case 2 and Case 3 highlights the significant impact of calibration methodologies on the representation of building energy dynamics. This finding underscores the importance of selecting appropriate calibration approaches to ensure reliable predictions of thermal performance and energy demand. Accurate capture of heat exchange behavior is vital for model applications, such as optimizing energy efficiency measures, evaluating design modifications, and supporting decision making for sustainable building operations.

In conclusion, implementing a detailed calibration that minimizes errors in both surface and zone temperatures, along with precise adjustments of thermal and convective properties, results in a more accurate and reliable model. These findings underscore the importance of advanced calibration methodologies for optimizing energy simulations in buildings.

CRediT authorship contribution statement

M. Cecilia Demarchi: Writing-review & editing, Formal analysis, Software. Sofía Gervaz Canessa: Writing, Formal analysis. Gabriel Pena. Writing, Formal analysis. Alejandro E. Albanesi: Methodology, Software, Supervision, Funding acquisition. Federico Favre: Writing, Methodology, Supervision, Funding acquisition.

Declaration of competing interest

The authors declare that they have no known competing financial interests or personal relationships that could have appeared to influence the work reported in this paper.

Acknowledgments

The authors gratefully acknowledge the financial support from CONICET (Argentine Council for Scientific and Technical Research) and the National Technological University of Argentina (UTN) for Grants PID ASECBFE0008389TC and ASECBFE0008366TC. They also gratefully acknowledge MEVIR for providing the construction details of the studied dwelling and for facilitating access to the site from the completion of construction until its delivery, enabling the execution of on-site measurements. M. C. Demarchi also acknowledges the Montevideo Group Association of Universities (AUGM) for the Postgraduate Mobility Scholarship.

References

[1] Asadi, S., Mostavi, E., Boussaa, D., Indraganti, M., 2019. Building energy model calibration using automated optimization-based algorithm. Energy and Buildings, Volume 198, Pages 106-114, ISSN 0378-7788 doi:https://doi.org/10.1016/j.enbuild.2019.06.001.

[2] Ascione, F., Bianco, N., Bottcher, O., Kaltenbrunner, R., Vanoli, G.P., 2016. Net zero-energy buildings in germany: Design, model calibration and lessons learned from a case-study in berlin. Energy and Buildings 133, 688–710. doi:https://doi.org/10.1016/j.enbuild.2016.10.019.

[3] Ascione, F., Bianco, N., Iovane, T., Mauro, G.M., Napolitano, D.F., Ruggiano, A., Viscido, L., 2020. A real industrial building: Modeling, calibration and pareto optimization of energy retrofit. Journal of Building Engineering, Volume 29, 101186, ISSN 2352-7102 doi:https://doi.org/10.1016/j.jobe.2020.101186.

[4] Baba, F.M., Ge, H., Zmeureanu, R., Wang, L.L., 2022. Calibration of building model based on indoor temperature for overheating assessment using genetic algorithm: Methodology, evaluation criteria, and case study. Building and Environment,Volume 207,Part B, 108518,ISSN 0360-1323 doi:https://doi.org/10.1016/j.buildenv.2021.108518.

[5] Beaulac, A., Lalonde, T., Haillot, D., Monfet, D., 2024. Energy modeling, calibration, and validation of a small-scale greenhouse using trnsys. Applied Thermal Engineering,Volume 248,Part A, 123195,ISSN 1359-4311 doi:https://doi.org/10.1016/j.applthermaleng.2024.123195.

[6] Cacabelos, A., Eguía, P., Febrero, L., Granada, E., 2017. Development of a new multi-stage building energy model calibration methodology and validation in a public library. Energy and Buildings,Volume 146,Pages 182-199,ISSN 0378-7788 doi:https://doi.org/10.1016/j.enbuild.2017.04.071.

[7] Chai, T., Draxler, R., 2014. Root mean square error (rmse) or mean absolute error (mae)?– arguments against avoiding rmse in the literature. geoscientific model development. Geoscientific Model Development doi:https://doi.org/10.5194/gmd-7-1247-2014.

[8] Chong, A., Augenbroe, G., Yan, D., 2021. Occupancy data at different spatial resolutions: Building energy performance and model calibration. Applied Energy,Volume 286,116492,ISSN 0306-2619 doi:https://doi.org/10.1016/j.apenergy.2021.116492.

[9] Cipriano, J., Mor, G., Chemisana, D., Pérez, D., Gamboa, G., Cipriano, X., 2015. Evaluation of a multi-stage guided search approach for the calibration of building energy simulation models. Energy and Buildings 87, 370–385. URL: https://www.sciencedirect.com/science/article/pii/S0378778814009013, doi:https://doi.org/10.1016/j.enbuild.2014.08.052.

[10] Darko, P., Štajduhar Ivan, Sandi, L., Igor, W., 2023. Development, calibration, and validation of a simulation model for indoor temperature prediction and hvac system fault detection. Buildings,Volume 13,ISSN 2075-5309 doi:https://www.mdpi.com/2075-5309/13/6/1388.

[11] Deb, K., 2001. Multiobjective optimization using evolutionary algorithms .

[12] Deb, K., Pratap, A., Agarwal, S., Meyarivan, T., 2002. A fast and elitist multiobjective genetic algorithm: Nsga-ii. IEEE Transactions on Evolutionary Computation 6, 182 – 197. doi:10.1109/4235.996017.

[13] Deep, K., Singh, K.P., Kansal, M., Mohan, C., 2009. A real coded genetic algorithm for solving integer and mixed integer optimization problems. Applied Mathematics and Computation 212, 505–518. doi:https://doi.org/10.1016/j.amc.2009.02.044.

[14] DOE2, . https://www.doe2.com/.

[15] Donovan, A.O., Sullivan, P.D.O., Murphy, M.D., 2019. Predicting air temperatures in a naturally ventilated nearly zero energy building: Calibration, validation, analysis and approaches. Applied Energy,Volume 250, Pages 991-1010,ISSN 0306-2619 doi:https://doi.org/10.1016/j.apenergy.2019.04.082.

[16] adn E. Mussatti, G.A., Ferrari, F., Muscio, A., 2018. A calibration methodology for building dynamic models based on data collected through survey and billings. Energy and Buildings,Volume 158, Pages 406-416,ISSN 0378-7788 doi:https://doi.org/10.1016/j.enbuild.2017.09.089.

[17] Energy, U.D.O., 2008. M&V guidelines: Measurement and Verification For Federal Energy Projects Version 3.0.

[18] EnergyPlus, . https://energyplus.net/.

[19] EVO, E., 2018. International performance measurement and verification protocol (IPMVP). Repéré à URL: https://evo-world.org/en/products-services-mainmenu-en/protocols/ipmvp.

[20] Fernandes, M.S., Rodrigues, E., Costa, J.J., 2022. A new wind direction-driven heat convection model is needed in dynamic simulation: What, why, and how. Energy and Buildings 256, 111716. doi:https://doi.org/10.1016/j.enbuild.2021.111716.

[21] Fortin, F.A., De Rainville, F.M., Gardner, M.A.G., Parizeau, M., Gagné, C., 2012. Deap: Evolutionary algorithms made easy. The Journal of Machine Learning Research 13, 2171–2175.

[22] Gervaz, S., Favre, F., 2024. Identifying key parameters in building energy models: Sensitivity analysis applied to residential typologies. Buildings 14. doi:10.3390/buildings14092804.

[23] Giuliani, M., Henze, G.P., Florita, A.R., 2016. Modelling and calibration of a high-mass historic building for reducing the prebound effect in energy assessment. Energy and Buildings,Volume 116,Pages 434-448,ISSN 0378-7788 doi:https://doi.org/10.1016/j.enbuild.2016.01.034.

[24] González, V., Bandera, C., 2022. A building energy models calibration methodology based on inverse modelling approach. Building Simulation .

[25] Guyot, D., Giraud, F., Simon, F., Corgier, D., Marvillet, C., Tremeac, B., 2020. Building energy model calibration: A detailed case study using sub-hourly measured data. Energy and Buildings 223, 110189. URL: https://www.sciencedirect.com/science/article/pii/S0378778820300505, doi:https://doi.org/10.1016/j.enbuild.2020.110189.

[26] Gómez, A.P., Draper, M., Favre, F., 2023. Modeling the convection coefficient with energyplus and its effects on a energy simulation of a typical uruguayan household.

[27] Haberl, J., Claridge, D.E., Culp, C., 2005. ASHRAE's Guideline 14-2002 for Measurement of Energy and Demand Savings: How to Determine what was really saved by the retrofit.

[28] Harshalatha, Patil, S., Kini, P.G., 2024. Calibration of simulation model to analyze hospital building energy performance. Energy and Buildings,Volume 313, 114242,ISSN 0378-7788 doi:https://doi.org/10.1016/j.enbuild.2024.114242.

[29] Herbinger, F., adn Michaël Kummert, C.V., 2023. Building energy model calibration using a surrogate neural network. Energy and Buildings,Volume 289, 113057,ISSN 0378-7788 doi:https://doi.org/10.1016/j.enbuild.2023.113057.

[30] IEA2023, . IEA (2023), World Energy Outlook 2023, IEA, Paris https://www.iea.org/reports/world-energy-outlook-2023?language=es, Licence: CC BY 4.0 (report); CC BY NC SA 4.0 (Annex A).

[31] Kim, Y., Heidarinejad, M., Dahlhausen, M., Srebric, J., 2017. Building energy model calibration with schedules derived from electricity use data. Applied Energy doi:https://doi.org/10.1016/j.apenergy.2016.12.167.

[32] Kounni, A.E., Outzourhit, A., Mastouri, H., Radoine, H., 2023. Building energy model automated calibration using pymoo. Energy and Buildings,Volume 298,113524,ISSN 0378-7788 doi:https://doi.org/10.1016/j.enbuild.2023.113524.

[33] Kunwar, N., Cetin, K.S., Passe, U., 2021. Calibration of energy simulation using optimization for buildings with dynamic shading systems. Energy and Buildings,Volume 236,110787,ISSN 0378-7788 doi:https://doi.org/10.1016/j.enbuild.2021.110787.

[34] Li, W., Tian, Z., Lu, Y., Fu, F., 2018. Stepwise calibration for residential building thermal performance model using hourly heat consumption data. Energy and Buildings,Volume 181, Pages 10-25,ISSN 0378-7788 doi:https://doi.org/10.1016/j.enbuild.2018.10.001.

[35] Lozinsky, C.H., Touchie, M.F., 2018. Improving energy model calibration of multi-unit residential buildings through component air infiltration testing. Building and Environment,Volume 134,218-229,ISSN 0360-1323 doi:https://doi.org/10.1016/j.buildenv.2018.02.040.

[36] Markel, A., Silvia, P.B., Anna, F.L., Xabat, O., 2024. Opportunities and barriers of calibrating residential building performance simulation models using monitored and survey-based occupant behavioural data: A case study in northern spain. Buildings,Volume 14,ISSN 2075-5309 doi:https://www.mdpi.com/2075-5309/14/7/1911.

[37] Mendes, V.F., Cruz, A.S., Gomes, A.P., Mendes, J.C., 2024. A systematic review of methods for evaluating the thermal performance of buildings through energy simulations. Renewable and Sustainable Energy Reviews,Volume 189,Article 113875,ISSN 1364-0321 doi:https://doi.org/10.1016/j.rser.2023.113875.

[38] Mirsadeghi, M., Cóstola, D., Blocken, B., Hensen, J.L.M., 2013. Review of external convective heat transfer coefficient models in building energy simulation programs: Implementation and uncertainty. Applied Thermal Engineering 56, 134–151. doi:https://doi.org/10.1016/j.applthermaleng.2013.03.003.

[39] no, S.M.M., Eguía-Oller, P., Granada-Álvarez, E., Erkoreka-González, A., 2021. Simulation and validation of indoor temperatures and relative humidity in multi-zone buildings under occupancy conditions using multi-objective calibration. Building and Environment,Volume 200, 107973,ISSN 0360-1323 doi:https://doi.org/10.1016/j.buildenv.2021.107973.

[40] Nouri, A., Frisch, J., van Treeck, C., 2021a. Statistical methodologies for verification of building energy performance simulation. doi:10.26868/25222708.2021.30538.

[41] Nouri, A., Frisch, J., van Treeck, C., 2021b. Statistical methodologies for verification of building energy performance simulation, in: Proceedings of the Building Simulation.

[42] Orme, M., Liddament, M.W., Wilson, A., 1998. Numerical Data for Air Infiltration and Natural Ventilation Calculations.

[43] Pachano, J.E., Bandera, C.F., 2021. Multi-step building energy model calibration process based on measured data. Energy and Buildings,Volume 252, 111380,ISSN 0378-7788 doi:https://doi.org/10.1016/j.enbuild.2021.111380.

[44] Pachano, J.E., Iglesias, M.F.V., Saiz, J.C., Bandera, C.F., 2023. Two-stage multi-step energy model calibration of the cooling systems of a large-space commercial building. Applied Thermal Engineering,Volume 230,Part A,120638,ISSN 1359-4311 doi:https://doi.org/10.1016/j.applthermaleng.2023.120638.

[45] Paliouras, P., N. Matzaflaras, R.P., Kolarik, J., 2015. Using measured indoor environment parameters for calibration of building simulation model- a passive house case study. Energy Procedia, Volume 78, Pages 1227-1232, ISSN 1876-6102 doi:https://doi.org/10.1016/j.egypro.2015.11.209.

[46] Peinturier, L., Wallom, D., 2024. Using an evidence-based approach to improve calibration of non-domestic building digital twins, in: 2024 7th International Conference on Energy Conservation and Efficiency (ICECE), pp. 1–6. doi:https://doi.org/10.1109/ICECE61222.2024.10505286.

[47] Perez, R., Jansen, P., Martins, 2012. pyopt: a python-based object-oriented framework for nonlinear constrained optimization. Struct Multidisc Optim 45, 101 – 118. doi:https://doi.org/10.1007/s00158-011-0666-3.

[48] Royapoor, M., Roskilly, T., 2015. Building model calibration using energy and environmental data. Energy and Buildings,Volume 94,Pages 109-120,ISSN 0378-7788 doi:https://doi.org/10.1016/j.enbuild.2015.02.050.

[49] Ruiz, G.R., Bandera, C.F., Temes, T.G.A., Gutierrez, A.S.O., 2016. Genetic algorithm for building envelope calibration. Applied Energy,Volume 168, Pages 691-705,ISSN 0306-2619 doi:https://doi.org/10.1016/j.apenergy.2016.01.075.

[50] TRNSYS, . https://www.trnsys.com/.

[51] de Wilde, P., 2014. The gap between predicted and measured energy performance of buildings: A framework for investigation. Automation in Construction,Volume 41,40-49,ISSN 0926-5805 doi:https://doi.org/10.1016/j.autcon.2014.02.009.

[52] Yin, R., Kiliccote, S., Piette, M.A., 2018. Linking measurements and models in commercial buildings: A case study for model calibration and demand response strategy evaluation. Energy and Buildings,Volume 124,222-235,ISSN 0378-7788 doi:https://doi.org/10.1016/j.enbuild.2015.10.042.

[53] Yun, G.Y., Song, K., 2017. Development of an automatic calibration method of a vrf energy model for the design of energy efficient buildings. Energy and Buildings,Volume 135, Pages 156-165,ISSN 0378-7788 doi:https://doi.org/10.1016/j.enbuild.2016.11.060.

[54] Zhang, Q., Tian, Z., Ma, Z., Li, G., Lu, Y., Niu, J., 2020. Development of the heating load prediction model for the residential building of district heating based on model calibration. Energy 205, 117949. URL: https://www.sciencedirect.com/science/article/pii/S0360544220310562, doi:https://doi.org/10.1016/j.energy.2020.117949.

[55] Zuhaib, S., Hajdukiewicz, M., Goggins, J., 2019. Application of a staged automated calibration methodology to a partially-retrofitted university building energy model. Journal of Building Engineering,Volume 26,100866,ISSN 2352-7102 doi:https://doi.org/10.1016/j.apenergy.2016.12.167.